Multirotor attitude control based on dexterous manipulator motion

Antun Ivanovic, Marko Car, Tomislav Haus, Matko Orsag and Stjepan Bogdan

***Abstract*— This paper addresses the issues of aerial manipulation concerning dynamic center of mass variations by deriving a control principle capable of exploiting disturbance as a means to stabilize the UAV. A complete mathematical model of an aerial robot consisting of rotorcraft UAV body and a generic multiple degree of freedom manipulator is provided. A coupled control scheme utilizing both rotor speed control and mass distribution using the mid-ranging approach is disseminated. We present the extensive simulation result using an example use case aerial robot. Finally, we present the experimental results for an aerial robot consisting of two moving masses distributed in a standard plus configuration in order to compare our proposed control paradigm with standard multirotor attitude control.**

I. INTRODUCTION

With interest in unmanned aerial vehicles growing rapidly over the course of last decade, aerial manipulation has become one of the most prominent research fields of robotics. Application scenarios include contact based inspection [1], transportation and assembly [2] and even complex interaction tasks involving opening doors [3] or turning valves [4]. Since the very beginning of aerial manipulation, payload has been observed as a disturbance to the autopilot control system relying on the rotors to stabilize the aircraft. Pounds et al. explored the effect added payload and the corresponding shift in the center of mass have on the stability of a standard linear PID attitude controller [5]. In [6] authors proposed an adaptive control approach to solve the problem of dynamic variations in the center of mass while transporting additional load. In [7] we analyzed the variable moment of inertia caused through motion of a multi degree of freedom manipulator. A common denominator of the state-of-the-art is that it observes a payload as a disturbance to the classical control approach of rotorcraft aerial vehicles.

In this paper we seek to invert this observation and use a controller capable of utilizing centroid variations in order to actively control the attitude of the aerial robot. This in turn enables us to use the payload to help stabilize the Unmanned Aerial System's (UAS) body. As the rotorcraft design increases payload-to-weight ratio, the center of mass becomes ever more dominant dynamic component of the system. The ability to utilize it as a control mechanism, rather than a control disturbance, could potentially help improve overall UAS performance. This is in line with our long term goal within the MORUS project [8], where we aim to build an unmanned aerial vehicle powered with four internal combustion engines (ICE), weighting 30kg in total and capable of lifting a 50kg heavy unmanned underwater vehicle (UUV). In order to solve the inherent problem of slow dynamics of ICE powered rotors, in [9] we proposed using a Moving Mass Control (MMC) concept. Similar concept was reported in [10] used on a coaxial helicopter vehicle.

Authors are with Faculty of Electrical and Computer Engineering, University of Zagreb, 10000 Zagreb, Croatia (antun.ivanovic, marko.car, tomislav.haus, matko.orsag, stjepan.bogdan) at fer.hr

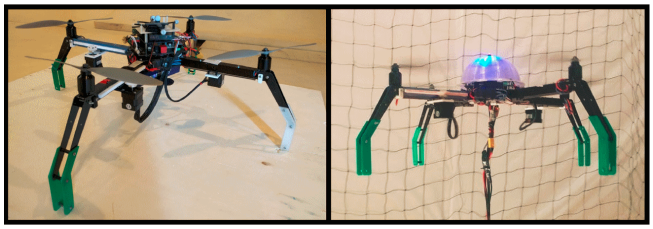

Fig. 1: Scaled down version of the MORUS UAV with moving mass control mechanism dubbed μMORUS. On right part of the image only two masses equipping a single axis can be observed. This setup was used in order to compare classical and the proposed control approaches. While on left image masses are on both axis. This setup was used in order to test MMC-VPC algorithm with position control.

Herein we will use a scaled model of the MORUS UAS shown in Fig. 1 and dubbed μMORUS, to demonstrate the effectiveness of the proposed control concept. Unlike in [10], μMORUS has four rotors which are used together with moving masses in order to stabilize the vehicle. We combine these two control concepts through a paradigm known as mid-ranging control. This paradigm has been introduced in process industry for plant control with multiple actuators working simultaneously [11],[12]. In recent years, this type of control has gained attention in robotics, in particular for position control of a robotic arm consisted of a macro and mini manipulator [13], [14]. We further extended the results from [9] by analyzing stability of the mid-ranging control concept, as well as applying such a control scheme on a multirotor UAV [15].

CONTRIBUTIONS!!!!!! Moreover, in this paper we aim to derive a generalized mathematical model that can be applied to a generic aerial robot consisting of a UAV body and a multi degree of freedom manipulator potentially carrying a payload.

The paper is organized as follows. We start by deriving a

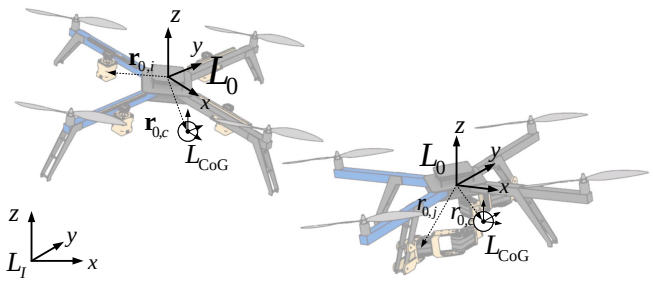

Fig. 2: We are considering two types of joints, prismatic and revolute. In both situations, the mass of the link is considered to be concentrated in the motor of the joint. This simplification is justified through the actual construction of the aerial robot, which tends to limit the payload of the manipulator, and thus uses lightweight link construction.

complete mathematical model of an aerial robot consisting of rotorcraft UAV body, and a generic multiple degree of freedom manipulator. Next we present the proposed, combined control system based on mid-ranging paradigm, Valve Position Control (VPC), utilizing both classical rotor and moving mass control concepts. Furthermore, we present the simulation results of a dual arm aerial robot with RR manipulators carrying an object. Finally, we present the experimental results for the μMORUS UAS. To compare the proposed control paradigm with classical approach single axis of the UAS is equipped with moving masses.

II. Mathematical model

Throughout the paper, all the vectors are expressed in the moving reference frame, i.e. the quadrotor body frame denoted as L_o in Fig. 2, with an exception of the gravity force vector which is conveniently express in the inertial frame L_I. Attached to the aerial robot's centorid (i.e. Center of Gravity CoG) is the coordinate frame L_{CoG} which is aligned with L_o. Careful reader should note that both angular momentum and angular velocities are obtained w.r.t. the vehicle's CoG, i.e. L_{CoG} frame. We use the following notation for radius and velocity vectors: $\boldsymbol{r}_{i,j}$ denotes radius vector from the L_i frame to the L_j and similar applies to the velocity $\boldsymbol{v}_{i,j}$ of the L_j frame w.r.t. the L_i frame.

We start the derivation with the CoG of the vehicle observed in the body frame which is given by:

$$\boldsymbol{r}_{0,c} = \frac{m_b \boldsymbol{r}_{0,b} + \sum_{i=1}^{n} m_i \boldsymbol{r}_{0,i}}{m_b + \sum_{i=1}^{n} m_i} = \frac{\sum_{i=1}^{n} m_i \boldsymbol{r}_{0,i}}{M}, \tag{1}$$

where m_b is the mass of the quadrotor rigid body (without moving masses), m_i denotes the mass of each manipulator link, M is the total mass of the vehicle, $\boldsymbol{r}_{0,i}$ represents the position of the i-th link's mass expressed in the body frame and n stands for the number of moving body parts (i.e. manipulator links). Note that by design the origin of the body frame L_0 coincides with the CoG of the quadrotor rigid body (i.e. the frame without the manipulator), which yields $\boldsymbol{r}_{0,b} = 0$.

In this analysis the links' masses are considered to be concentrated in the DC motor driven joints of the manipulator, as shown in Fig. 3. This is due to the nature of constructing an aerial manipulator with limited payload capabilities. Each link of the aerial robot is observed having its own linear momentum $\mathbf{L}_i$:

$$\begin{aligned} \mathbf{L}_i =& m_i \left(\mathbf{V}_0 + \mathbf{v}_{0,i} + \boldsymbol{\omega}_i \times \mathbf{r}_{0,i} \right) \\ =& m_i \left(\mathbf{V}_c - \mathbf{v}_{0,c} + \mathbf{v}_{0,i} + (\boldsymbol{\Omega} + \boldsymbol{\omega}_{0,i}) \times \mathbf{r}_{c,i} \right), \end{aligned} \tag{2}$$

where $\mathbf{V}_0$, $\mathbf{V}_c$, $\boldsymbol{\omega}_i$ and $\boldsymbol{\Omega}$ represent linear velocity of the i-th frame, linear velocity of CoG, angular velocity of the body part and angular velocity of body, respectively. Furthermore, $\boldsymbol{\omega}_{0,i}(q_1, ..., q_{i-1})$ is a function of manipulator joints that affect the rotation of the i-th body part.

Similarly, one can write the equations for the angular momentum of the i-th body part $\mathbf{H}_i$:

$$\mathbf{H}_i = \mathbf{I}_i^c \boldsymbol{\omega}_i + \mathbf{r}_{c,i} \times m_i \mathbf{v}_{c,i}, \tag{3}$$

with $\mathbf{I}_i^c$ denoting the moment of inertia of the i-th link w.r.t. the CoG. To compute these moments of inertia we apply the Parallel axis theorem:

$$\mathbf{I}_i^c = \mathbf{I}_i + m_i \left(r_{c,i}^T \cdot r_{c,i} \mathbf{E}_{3\times 3} - r_{c,i} \cdot r_{c,i}^T \right) \tag{4}$$

using $\mathbf{E}_{3\times 3}$ to denote a 3×3 identity matrix.

Applying basic Newton laws of motion allows one to combine the change of linear and angular momentum w.r.t. the forces and torques applied on each object i:

$$\begin{aligned} \frac{\partial^{\omega_i}}{\partial t} \mathbf{L}_i &= \underbrace{-m_i g \hat{\mathbf{z}}}_{\text{gravity}} + \xi_i \underbrace{K_{m_i} U_i \hat{\mathbf{z}}_i}_{\text{motor force}} + \underbrace{c_{d_i} \mathbf{v}_{0,i}}_{\text{friction}} \\ \frac{\partial^{\omega_i}}{\partial t} \mathbf{H}_i &= (1 - \xi_i) \underbrace{K_{m_i} U_i \hat{\mathbf{z}}_i}_{\text{motor torque}} . \end{aligned} \tag{5}$$

In previous equations we used $\frac{\partial^{\omega_i}}{\partial t}$ to denote the time derivative w.r.t. a moving (i.e. rotating) frame. Unit vectors $\hat{\mathbf{z}}$ and $\hat{\mathbf{z}}_i$ denote the z axis of the inertial and i-th frame, respectively. Furthermore, g denotes the gravity constant, U_i is the voltage applied to i-th motor and K_{m_i} denotes the i-th motor constant. Finally, we use $\xi_i = 1$ to denote if the joint is prismatic, or revolute $\xi_i = 0$.

It can easily be shown that, since we observe the forces w.r.t. the CoG of the system and each body part respectively, the moment due to gravity is equal to zero. So far we have observed each moving part of the aerial manipulator separately. Next we proceed to observe the system as a whole, and continue to derive the linear momentum of the whole system $\mathbf{L}_s$:

$$\mathbf{L}_s = \mathbf{L}_b + \sum_{i=1}^{n} \mathbf{L}_i = M \left(\mathbf{V}_0 + \boldsymbol{\Omega} \times \mathbf{r}_{0,c} \right) + \sum_{i=1}^{n} \mathbf{L}_{0,i}, \tag{6}$$

where $\mathbf{L}_b$ denotes the linear momentum of the quadrotor body. The same can, of course, be derived for the angular

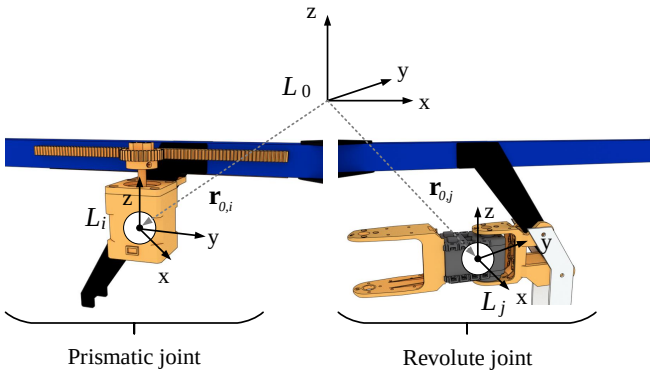

Fig. 3: We are considering two types of joints, prismatic and revolute. In both situations, the mass of the link is considered to be concentrated in the motor of the joint. This simplification is justified through the actual construction of the aerial robot, which tends to limit the payload of the manipulator, and thus uses lightweight link construction.

momentum of the system $\mathbf{H}_s$:

$$\mathbf{H}_s = \mathbf{H}_b + \sum_{i=1}^{n} \mathbf{H}_i = \mathbf{I}_s^c \boldsymbol{\Omega} + \sum_{i=0}^{n} \mathbf{r}_{c,i} \times m_i \mathbf{v}_{c,i} + \sum_{i=1}^{n} \mathbf{I}_i^c \omega_{0,i}, \tag{7}$$

with $\mathbf{H}_b$ denoting the angular momentum of the quadrotor rigid body and $\mathbf{I}_s^c$ is the total moment of inertia of the system w.r.t. CoG, obtained while taking into account the parallel axis theorem. Next it is straightforward to use the 2nd Newton law to derive the equations of motion, and model how gravity and propeller thrust intertwine to exert forces and torques on the system as a whole:

$$\frac{d^{\Omega}\mathbf{L}_s}{dt} = \sum_{j=1}^{4} \mathbf{F}_{r_j} + \mathbf{F}_g = \sum_{j=1}^{4} \underbrace{b_f \Omega_j^2 \hat{\mathbf{z}}_0}_{\text{thrust}} - \underbrace{Mg\hat{\mathbf{z}}}_{\text{gravity}} \tag{8}$$

$$\frac{d^{\Omega}\mathbf{H}_s}{dt} = \sum_{j=1}^{4} \boldsymbol{\tau}_{r_j} = \sum_{j=1}^{4} (\underbrace{\mathbf{r}_{c,j} \times \mathbf{F}_{r_j}}_{\text{thrust displacement}} + \underbrace{\zeta_j b_m b_f \Omega_j^2 \hat{\mathbf{z}}_0}_{\text{induced drag}}).$$

As one can observe in previous equations, we use standard nonlinear quadratic equation to derive the relationship between the rotor speed Ω_j and the thrust applied to the quadrotor. Symbols b_f and b_m denote the aerodynamic coefficients, while $\zeta_j = 1$ denotes clockwise rotating blades and $\zeta_j = -1$ denotes counterclockwise rotation.

In this paper we concentrate our efforts on the problem of attitude control. In order to hover one is required to maintain $\frac{d^{\Omega}\mathbf{H}_s}{dt} = 0$. To derive the necessary equations, we adopt the standard hovering assumption and neglect the second order dynamics. Furthemore, we introduce a $3 \times n$ Jacobian matrix $\mathbf{J}_{0,i}$ that relates the linear motion of each body $\dot{\mathbf{r}}_{0,i}$ with the motion of the joints $\dot{\mathbf{q}}$. With these notations and simplifications in mind and through Laplace tansform, we write the final nonlinear vector equation:

$$\mathbf{I}_s^c \boldsymbol{\Theta} s^2 = \mathbf{g}_1(s, \mathbf{r}_{0,c}(\mathbf{q})) + \mathbf{g}_2(s, \sum_{j=1}^{4} \boldsymbol{\tau}_{r_j}) \tag{9}$$

In (9) we introduced $\boldsymbol{\Theta}$, as the attitude vector, which through the aforementioned hover assumptions can be considered equal to Euler angles of the system. We have separated both classical rotor control $\mathbf{g}_2$ and moving mass CoG control $\mathbf{g}_1$ dependent on the motion of the manipulator $\mathbf{r}_{0,c}(\mathbf{q})$. Since there is no qualitative distinction between $\mathbf{g}_2$ and standard quadrotor control, it will not be considered further in the text. However, careful reader should note non minimum phase dynamics caused through the motion of the arms $\ddot{\mathbf{q}}$ in $\mathbf{g}_1$:

$$\mathbf{g}_1 = M\mathbf{r}_{0,c}(\mathbf{q}) \times \mathbf{g} - \sum_{i=0}^{n} m_i \mathbf{r}_{c,i}(\mathbf{q}) \times \mathbf{J}_{0,i}(\mathbf{q}) \mathbf{q} s^2. \tag{10}$$

The non minimum phase dynamics can be clearly observed in a linearized model of the equation. For more details we refer the reader to [9]. In the remaining sections of the paper we will consider scalar transfer functions G_1 and G_2 linearized with an assumption of near hover conditions, observing only pitch angle for clarity:

$$\begin{aligned} \Theta(s) =& G_1(s) x_c + G_2(s) \Delta\Omega_{\sum} \\ =& \frac{\widehat{\mathbf{g}_1(s, \mathbf{r}_{0,c}(\mathbf{q}))}}{I_{s\,yy}^c s^2} x_c + \frac{\widehat{\mathbf{g}_2(s, \sum_{j=1}^{4} \boldsymbol{\tau}_{r_j})}}{I_{s\,yy}^c s^2} \Delta\Omega_{\sum}, \end{aligned} \tag{11}$$

where we used $\widehat{(\cdot)}$ to denote the linearization, x_c as x-axis component of $\mathbf{r}_{0,c}$ and $\Delta\Omega_{\sum}$ as the rotor speed control inputs.

III. Mid-ranging control concept

In this section we present a mid-ranging controller concept which utilizes both CoG positioning and rotors' variations to control vehicle's attitude. We propose to use a structure based on the Valve Position Control (VPC) concept [12]. The concept is named after a liquid flow control problem with a small and a big valve, where a big valve can produce higher flow than a small valve, but with less precision and slower response [11]. On the other hand, using only a small valve often results in actuator saturation and inability to satisfy flow capacities. VPC based control algorithm manipulates both valves to track desired flow level while keaping steady state value of the small valve at given setpoint.

For the MORUS UAS roll/pitch control concept, moving masses are considered as a small valve, while the rotors represent the big valve. We have shown in [9] that the MMC based control has higher bandwidth than the control based on rotors powered by IC engines. We also claim that rolling/pitching torques can be controlled with higher precision through MMC than with rotors' variations, since the MMC concept idealy controls the position of the CoG in a millimeter range. On the other hand, the torque that can be produced by rotors' variations is much larger than the maximum torque

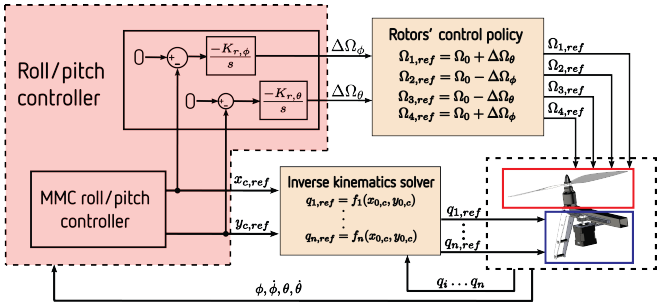

Fig. 4: The structure of the proposed MMC-VPC controller.

produced by shifting the CoG, which allows us to utilize it as the "big" valve. In the provided experimental results however, we use rotors powered by DC motors to emulate slow rotors and verify the proposed VPC concept.

In the proposed concept (Fig. 4), the main controller (MMC) manipulates the position of the moving masses in order to track roll/pitch references. In this paper we utilize a cascade P-P MMC controller whose design, based on root-locus analysis, is presented in [9]. Note that for the main controller we can utilize any type of MMC controller, e.g. state space controller presented in [16]. The auxiliary controller (VPC) generates references for rotors' variations with a goal to keep the steady state position of the moving mass mechanism in the middle of its operating range. Note that the reference for this controller is 0, which is considered as a neutral position in this paper. The feedback signal of the VPC controller is the reference position of the vehicle's CoG generated by the MMC controller.

In this paper we show important properties of the MMC-VPC controller for the linearized pitch dynamical model presented by transfer functions G_1 and G_2. These transfer functions present dynamical effect of the CoG variations and rotors variations to vehicle's pitch angle. If we denote by C_1 the main MMC controller and by C_2 the auxilliary VPC controller, the closed loop transfer function of the vehicle's pitch angle is given by:

$$G_{\theta,\theta_r}(s) = \frac{\theta(s)}{\theta_r(s)} = \frac{C_1(G_1 - C_2G_2)}{1 + C_1(G_1 - C_2G_2)}. \tag{12}$$

First, we compute the static gain of (12) to show that the MMC-VPC controller ensures zero static error given a reference:

$$\lim_{s->0} G_{\theta,\theta_r}(s) = \lim_{s->0} \frac{C_1}{\frac{1}{(G_1 - C_2G_2)} + C_1} = 1, \tag{13}$$

where we used $\lim_{s->0}(G_1 - C_2G_2) = \infty$, as the transfer functions G_1 and G_2 have infinite gain and C_2 is chosen as a negative I controller. As both G_1 and G_2 have positive gains, the gain of C_2 is chosen negative to ensure that the moments produced by CoG variations and rotors' variations have the same direction. Next, we compute closed loop transfer function of $x_{c,ref}(s)$ given an output reference $\theta_r(s)$ and its static gain:

$$\begin{aligned} G_{x_c,\theta_r}(s) = \frac{x_{c,ref}(s)}{\theta_r(s)} &= \frac{C_1}{1 + C_1(G_1 - C_2G_2)} \\ &= C_1(1 - G_{\theta,\theta_r}(s)), \qquad (14) \\ \lim_{s->0} G_{x_c,\theta_r}(s) &= 0. \qquad (15) \end{aligned}$$

Finally, we compute the transfer functions and static gains of the output value θ and CoG position referenxe $x_{c,ref}$ given an output disturbance d:

$$\begin{aligned} G_{\theta,d}(s) = \frac{\theta(s)}{d(s)} &= \frac{1}{1 + C_1(G_1 - C_2G_2)} \\ &= (1 - G_{\theta,\theta_r}(s)), \qquad (16) \\ \lim_{s->0} G_{\theta,d}(s) &= 0, \qquad (17) \\ G_{x_{c,ref},d}(s) = \frac{x_{c,ref}(s)}{d(s)} &= \frac{C_1}{1 + C_1(G_1 - C_2G_2)} \\ &= C_1(1 - G_{\theta,\theta_r}(s)), \qquad (18) \\ \lim_{s->0} G_{x_c,\theta_r}(s) &= 0. \qquad (19) \end{aligned}$$

The computed steady state gains prove that the proposed MMC-VPC structure ensures reference tracking and output disturbance rejection with zero steady CoG position, which allows the moving mass mechanism to work around the center point of this operating range.

To tune the controller gains we propose a two stage procedure. First, the gains of the cascade P-P controller are chosen according to [9], assuming that the output of the auxiliary controller is 0. Second, respecting gain limits from the Routh-Hurwitz analysis, the integral gain of the auxiliary controller is tuned to obtain desired, stable closed loop dynamics.

IV. Simulation

To validate the VPC concept with PID-based position controller on an arbitrary aerial manipulator we created realistic simulation environment in Gazebo simulator within Robot Operating System (ROS). We model the UAV a as single rigid body with rotating joints attached to each of four motor arms. Furthermore, each rotating joint has a propeller attached. In order to simulate rotor dynamics we use a plugin from open source *rotors_simulator* [17] package. We also equip the UAV with realistic sensors from *hector_gazebo* [18] to measure vehicle's attitude and pose.

To control the COG, moving mass is attached to each arm of the UAV with mass $m = 0.2kg$, while the central body of the UAV is considered to be a single rigid body. Standard PID control is utilized to move the masses along the arms of the UAV while restricting the workspace to $\Delta x \in [-0.08m, 0.08m]$. The aforementioned MMC-VPC concept is utilized to control attitude and cascade PID controller is used to control position. Two simulation experiments were conducted to validate the performance of the controller: hovering and trajectory following. The RMS measure is used to compare results.

While hovering for $t_h = 180s$, the UAS achieved position score $RMS_h = 0.00076m$. For the trajectory tracking, a square trajectory of side length $a = 1m$ was chosen as the example. A set of 10 identical trajectories were performed by the UAS, each lasting for $t = 20.89s$. Figure 5a depicts the trajectory tracking. The average position score over 10 trajectories was $RMS_{pos} = 0.2946m$. Figure 5b depicts pitch angle tracking performance. One can notice a very small delay while achieving great tracking of the reference, which can be backed up with $RMS_\theta = 0.0021°$. Similar result is obtained for roll angle with $RMS_\phi = 0.0019°$.

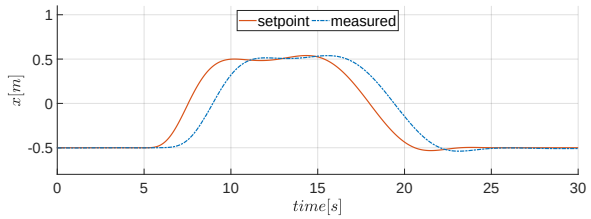

(a) Results obtained for x-axis while tracking square trajectory. Similar results were obtained for y-axis.

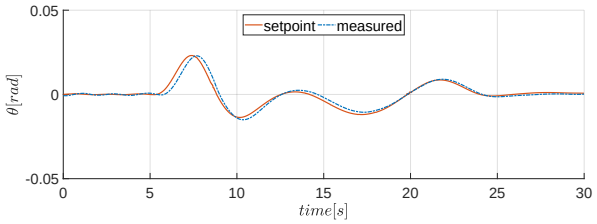

(b) Results obtained for pitch angle θ while tracking square trajectory. Similar results are obtained for roll angle.

Fig. 5

V. Experiments

To demonstrate the proposed MMC-VPC control algorithm in action, we present the results of several experiments conducted on a real physical platform μMORUS, shown in Fig. 1. Our aerial robot is a 3D Robotics quadrotor equipped with four moving masses (NEMA 14 stepper motors) with a rack and pinion mechanism that transform rotational motion into linear motion. Masses are placed on each arm of the μMORUS platform. At the same time rotors are symmetrically placed around the central body in a pattern known as plus (+) configuration. We use a custom designed printed circuit board to command stepper motors and Pixhawk PX4 as the flight controller. For out first experiment we wanted to compare MMC-VPC control algorithm and classical rotor speed control in stabilization flight. We implemented MMC-VPC for pitch angle control while classical algorithm was controlling the roll angle. The second experiment was conducted to test the controller performance on simple trajectory. For that case, the MMC-VPC algorithm is implemented for both axis together with position controller. All control algorithms are implemented on the Pixhawk PX4 flight controller and the off-board computer is used for data logging. For testing purposes μMORUS is powered over electric cables and connected to the off-board computer through a USB cable.

A. Manual stabilization flight

Our first experiment was manual stabilization flight with μMORUS. Pilot took-off with the vehicle, hovered for few minutes and then landed. Fig. 6a represents pitch and roll measurements during experiment. Considering attitude measurements in Fig. 6a, the results show that there is no significant difference between the two control paradigms. Results shows a stable flight, where both roll and pitch angles are within a few degrees. One has to be aware that the pilot was manually trying to keep the vehicle steady during the whole experiment, and that our goal was to show the proposed concept can stabilize the UAS in flight. The reference for MMC-VPC algorithm outputs, rotors 3 and 4, are given in Fig. 6b alongside rotor 1 and rotor 2 which are controlled using the standard attitude controller. One can notice that the rotors commanded with MMC-VPC operate in lower bandwith. This is in line with the expected results, since the moving masses control attitude during the transient period which requires faster motion. This results with smother rotors' references, when compared to rotors 1 and 2. Nevertheless, the response of the UAV remains the same, as shown in Fig. 6a. The parameter used for attitude control loop are given in Table I.

TABLE I: MMC-VPC controller gains for attitude control loop where.

	ϕ	$\dot{\phi}$	θ	$\dot{\theta}$	ψ	$\dot{\psi}$
KP	0	0	0	0	0	0
KI	0	0	0	0	0	0
KD	0	0	0	0	0	0
KI_{VPC}	0	0	0	0	0	0

B. Trajectory following

The second experiment was conduced in order to test MMC-VPC algorithm with higher level control. We implemented position control in the standard cascade control form with PID controller. To tune our position controller we started with parameters from simulation and with some fine tuning we reached parameters shown in Table II.

We can divide second experiment in to a two parts. The part a) of the experiment was to hover (maintain the constant position) with the μMORUS UAS and the part b) was to follow trajectory. On Fig. 7 is shown position setpoint and feedback of the UAS while hovering. The UAS was able to maintain constant position with RMS error for position in x-axis $RMS_X = 0.0739m$ and y-axis $RMS_Y = 0.0424m$. The low level controller states

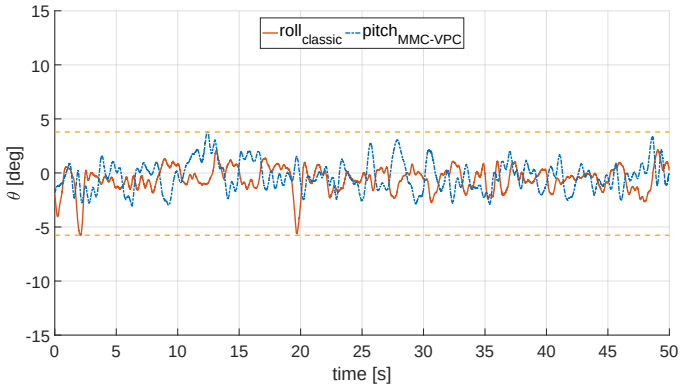

(a)

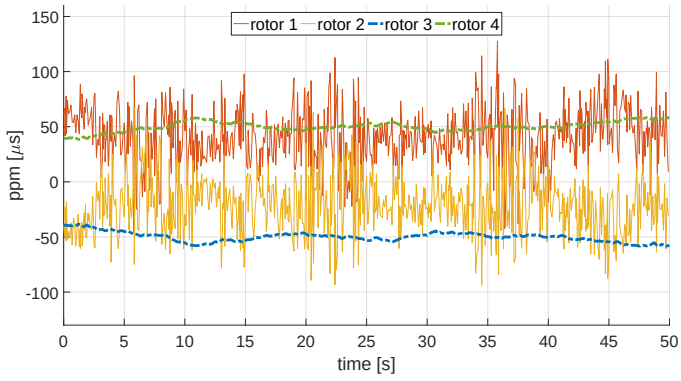

(b)

Fig. 6: Experimental results of μMORUS UAS in stabilization flight. Roll and pitch measurements are depicted in a). b) shows reference for rotors 1-4. MMC-VPC takes higher bandwidth out of rotor 3 and 4 control, which results with smoother rotors' reference when compared to classically controlled rotors 1 and 2.

TABLE II: PID controller gains for cascade position control where x, y and z denotes outer control loop (position) and vx, vy and vz denotes inner control loop (velocity).

	x	vx	y	vy	z	vz
KP	0	0	0	0	0	0
KI	0	0	0	0	0	0
KD	0	0	0	0	0	0

for roll axis are shown on Fig. 8, while pitch axis is almost identical. Here we can point out RMS error for roll angle $RMS_\phi = 2.091°$ and RMS error for pitch angle $RMS_\theta = 2.354°$.

The b) part of the experiment (following a trajectory) give us a position results that are shown on Fig. 9. The UAS was able to follow trajectory with RMS error $RMS = 0.3139m$. The roll angle and roll rate during the trajectory execution are shown on Fig. 10. The video showing both experiments can be found in [19]. The Github repository with source code for both simulation can bi found in [20] and experiments in [21].

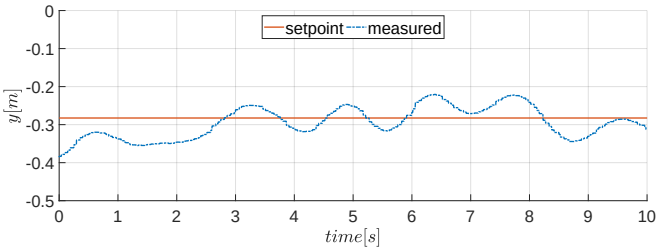

Fig. 7: Results of the hovering experiment. Figure shows position setpoint and measurement for y-axis. Similar results are obtained for x-axis.

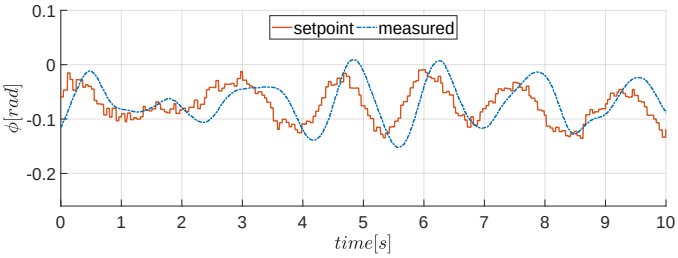

(a)

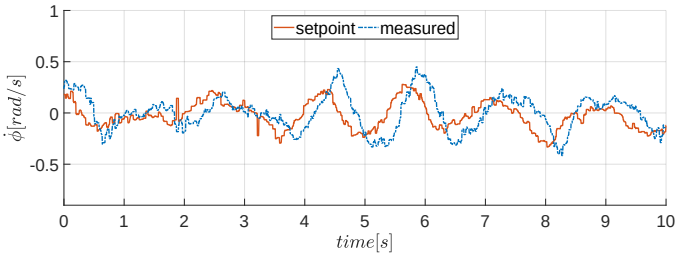

(b)

Fig. 8: The experimental results of the μMORUS UAS during hovering experiment. a) shows a setpoints and the corresponding measurements for angle ϕ. b) shows a setpoints and the corresponding measurements for angular velocity $\dot{\phi}$. The results for θ angle are similar.

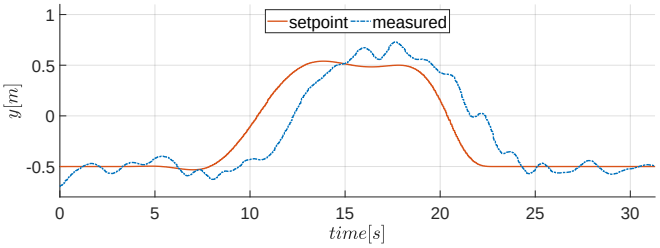

Fig. 9: Results of the trajectory following. Figure shows position setpoint and measurement for y-axis. Similar results are obtained for x-axis.

VI. Conclusion

ISPRAVITI!!!!!!!!!In this paper we proposed MMC-VPC attitude control for UAVs. The approach utilizes both shifting of the vehicle's CoG and variations of rotors' angular velocity. In simulation environment we successfully tested the proposed control strategy for quadcopter

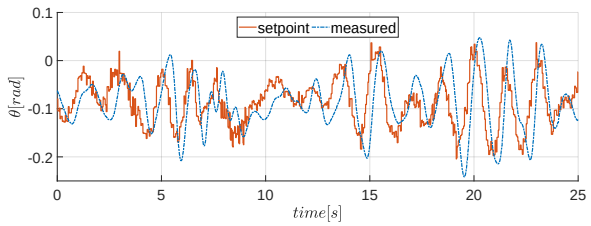

(a)

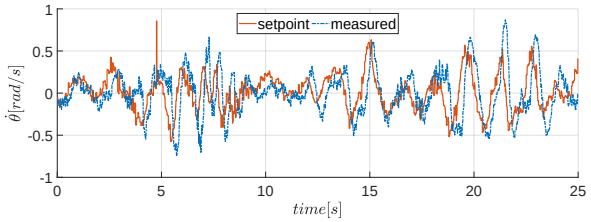

(b)

Fig. 10: The experimental results of the μMORUS UAS during the trajectory following experiment. a) shows a setpoints and the corresponding measurements for angle ϕ. b) shows a setpoints and the corresponding measurements for angular velocity $\dot{\phi}$. The results for θ angle are similar.

equipped with dual arm manipulator. We have shown that manipulator operates on higher bandwidth, changing the vehicle's CoG, thus enabling fast change of attitude. At the same time rotors operate on lower bandwidth, making sure the moving masses avoid saturation limits, which is one key benefit of this control strategy. In experimental setup, we tested the control approach on μMORUS UAV during several successful flights, and showed the results which are comparable to the standard rotor based attitude control. Furthemore, the results comply with the presented mathematical model and simulation results.

ACKNOWLEDGMENT

This research was supported in part by NATO's Emerging Security Challenges Division in the framework of the Science for Peace and Security Programme as Multi Year Project under G. A. number 984807, named Unmanned system for maritime security and environmental monitoring - MORUS.

References

[1] K. Alexis, G. Darivianakis, M. Burri, and R. Siegwart, "Aerial robotic contact-based inspection: planning and control," *Autonomous Robots*, vol. 40, no. 4, pp. 631–655, 2016.

[2] A. E. Jimenez-Cano, J. Martin, G. Heredia, A. Ollero, and R. Cano, "Control of an aerial robot with multi-link arm for assembly tasks," in *Proceedings - IEEE International Conference on Robotics and Automation*, pp. 4916–4921, IEEE, 5 2013.

[3] H. Tsukagoshi, M. Watanabe, T. Hamada, D. Ashlih, and R. Iizuka, "Aerial manipulator with perching and door-opening capability," in *2015 IEEE International Conference on Robotics and Automation (ICRA)*, pp. 4663–4668, 2015.

[4] C. Korpela, M. Orsag, and P. Oh, "Towards valve turning using a dual-arm aerial manipulator," in *Intelligent Robots and Systems (IROS 2014), 2014 IEEE/RSJ International Conference on*, pp. 3411–3416, 2014.

[5] P. E. Pounds, D. R. Bersak, and A. M. Dollar, "Stability of small-scale UAV helicopters and quadrotors with added payload mass under PID control," *Autonomous Robots*, vol. 33, no. 1-2, pp. 129–142, 2012.

[6] I. Palunko and R. Fierro, "Adaptive control of a quadrotor with dynamic changes in the center of gravity," in *Proceedings 18th IFAC World Congress*, vol. 18, pp. 2626–2631, 2011.

[7] C. Korpela, M. Orsag, T. Danko, B. Kobe, C. McNeil, R. Pisch, and P. Oh, "Flight stability in aerial redundant manipulators," in *2012 IEEE International Conference on Robotics and Automation*, pp. 3529–3530, IEEE, 5 2012.

[8] "Morus project." `http://www.fer.unizg.hr/morus`. Accessed: 2017-09-08.

[9] T. Haus, M. Orsag, and S. Bogdan, "Mathematical Modelling and Control of an Unmanned Aerial Vehicle with Moving Mass Control Concept," *Journal of Intelligent and Robotic Systems: Theory and Applications*, 2017.

[10] C. Bermes, S. Leutenegger, S. Bouabdallah, D. Schafroth, and R. Siegwart, "New design of the steering mechanism for a mini coaxial helicopter," in *Intelligent Robots and Systems, 2008. IROS 2008. IEEE/RSJ International Conference on*, pp. 1236–1241, IEEE, 2008.

[11] B. J. Allison and A. J. Isaksson, "Design and Performance of Mid-Ranging Controllers," *IFAC Proceedings Volumes*, vol. 30, no. 9, pp. 523–528, 1997.

[12] B. J. Allison and S. Ogawa, "Design and tuning of valve position controllers with industrial applications," *Transactions of the Institute of Measurement and Control*, vol. 25, no. 1, pp. 3–16, 2003.

[13] O. Sornmo, B. Olofsson, A. Robertsson, and R. Johansson, "Adaptive internal model control for mid-ranging of closed-loop systems with internal saturation," *IEEE International Conference on Intelligent Robots and Systems*, pp. 4893–4899, 2013.

[14] Z. Ma, G. S. Hong, M. H. Ang, and A. N. Poo, "Mid-ranging control of a macro/mini manipulator," in *2015 IEEE International Conference on Advanced Intelligent Mechatronics (AIM)*, pp. 755–760, July 2015.

[15] T. Haus, A. Ivanovic, M. Car, M. Orsag, and S. Bogdan, "Mid-ranging control concept for a multirotor uav with moving masses," in *2018 26th Mediterranean Conference on Control and Automation (MED)*, June 2018.

[16] T. Haus, M. Orsag, and S. Bogdan, "A concept of a non-tilting multirotor-uav based on moving mass control," in *2017 International Conference on Unmanned Aircraft Systems (ICUAS)*, pp. 1618–1624, June 2017.

[17] F. Furrer, M. Burri, M. Achtelik, and R. Siegwart, *Robot Operating System (ROS): The Complete Reference (Volume 1)*, ch. RotorS—A Modular Gazebo MAV Simulator Framework, pp. 595–625. Cham: Springer International Publishing, 2016.

[18] J. Meyer, A. Sendobry, S. Kohlbrecher, U. Klingauf, and O. von Stryk, "Comprehensive simulation of quadrotor uavs using ros and gazebo," in *3rd Int. Conf. on Simulation, Modeling and Programming for Autonomous Robots (SIMPAR)*, p. to appear, 2012.

[19] "Laboratory for robotics and intelligent control systems youtube channel." `https://goo.gl/1PWUJ2`.

[20] "mmuav gazebo." `https://github.com/larics/mmuav_gazebo`, 2018.

[21] "px4-firmware." `https://github.com/larics/px4-firmware`, 2018.